JACS
JOURNAL OF THE AMERICAN CHEMICAL SOCIETY
Article
pubs.acs.org/JACS

Fluorinated Copolymer PCPDTBT with Enhanced Open-Circuit Voltage and Reduced Recombination for Highly Efficient Polymer Solar Cells

Steve Albrecht,[†] Silvia Janietz,[‡] Wolfram Schindler,[§] Johannes Frisch,[⊥] Jona Kurpiers,[†] Juliane Kniepert,[†] Sahika Inal,[†] Patrick Pingel,[†] Konstantinos Fostiropoulos,[§] Norbert Koch,[§,⊥] and Dieter Neher*[,†]

[†]Institut für Physik und Astronomie, Universität Potsdam, Karl-Liebknecht-Strasse 24-25, 14476 Potsdam, Germany
[‡]Fraunhofer Institut für Angewandte Polymerforschung, Geiselbergstrasse 69, 14476 Potsdam, Germany
[§]Helmholtz-Zentrum Berlin für Materialien und Energie GmbH, Hahn-Meitner-Platz 1, 14109 Berlin, Germany
[⊥]Institut für Physik, Humboldt-Universität zu Berlin, Brook-Taylor-Strasse 6, 12489 Berlin, Germany

Supporting Information

ABSTRACT: A novel fluorinated copolymer (F-PCPDTBT) is introduced and shown to exhibit significantly higher power conversion efficiency in bulk heterojunction solar cells with $PC_{70}BM$ compared to the well-known low-band-gap polymer PCPDTBT. Fluorination lowers the polymer HOMO level, resulting in high open-circuit voltages well exceeding 0.7 V. Optical spectroscopy and morphological studies with energy-resolved transmission electron microscopy reveal that the fluorinated polymer aggregates more strongly in pristine and blended layers, with a smaller amount of additives needed to achieve optimum device performance. Time-delayed collection field and charge extraction by linearly increasing voltage are used to gain insight into the effect of fluorination on the field dependence of free charge-carrier generation and recombination. F-PCPDTBT is shown to exhibit a significantly weaker field dependence of free charge-carrier generation combined with an overall larger amount of free charges, meaning that geminate recombination is greatly reduced. Additionally, a 3-fold reduction in non-geminate recombination is measured compared to optimized PCPDTBT blends. As a consequence of reduced non-geminate recombination, the performance of optimized blends of fluorinated PCPDTBT with $PC_{70}BM$ is largely determined by the field dependence of free-carrier generation, and this field dependence is considerably weaker compared to that of blends comprising the non-fluorinated polymer. For these optimized blends, a short-circuit current of 14 mA/cm^2, an open-circuit voltage of 0.74 V, and a fill factor of 58% are achieved, giving a highest energy conversion efficiency of 6.16%. The superior device performance and the low band-gap render this new polymer highly promising for the construction of efficient polymer-based tandem solar cells.

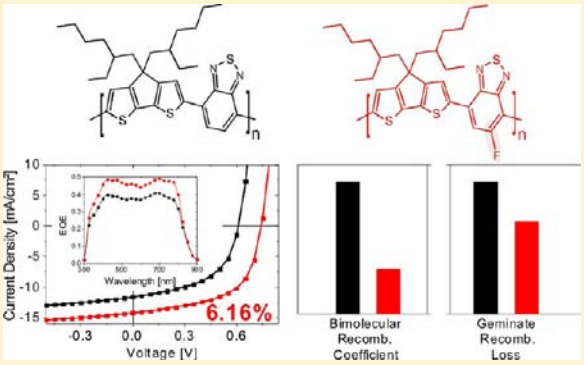

INTRODUCTION

A dramatic improvement in the efficiency of bulk heterojunction (BHJ) solar cells based on electron-donating conjugated polymers in combination with soluble fullerene derivatives has been achieved over the past 3 years. Certified power conversion efficiencies (PCEs) now reach 9% for single junctions and exceed the 10% benchmark for tandem solar cells.[1−3] This trend brightens the vision of organic photovoltaics becoming competitive with inorganic solar cells. Most such high-performance cells comprise donor−acceptor (DA) copolymers following the concept introduced by Wynberg and co-workers.[4] The introduction of adequate donor and acceptor units led to lower polymer highest molecular orbital (HOMO) energies for enhanced open-circuit voltage (V_{oc}) in blends with [6,6]-phenyl C_{70}-butyric acid methyl ester ($PC_{70}BM$).[5−8] In parallel, the copolymer band-gap was continuously reduced to improve matching of the polymer absorption with the sun spectrum, resulting in higher short-circuit currents (J_{sc}).[6,9,10] Control over the blend morphology has been achieved with the help of solvent additives.[6,10−13]

One of these copolymers is poly[2,6-(4,4-bis(2-ethylhexyl)-4*H*-cyclopenta[2,1-b;3,4-b′]dithiophene)-*alt*-4,7-(2,1,3-benzothiadiazole)] (PCPDTBT),[14] and its silicon- and germanium-bridged derivatives, PSBTBT[15,16] and PGe1-EH,[17] respectively. These polymers have low band-gaps of around 1.45 eV. Blends with $PC_{70}BM$ exhibit high external quantum efficiencies throughout the entire visible spectrum extending up to 800 nm, resulting in one of the highest J_{sc} values yet reported for BHJ single-junction cells[9,18] and PCEs of 4.5−5.5% for

Received: May 24, 2012
Published: August 6, 2012

   dx.doi.org/10.1021/ja305039j | *J. Am. Chem. Soc.* 2012, 134, 14932−14944

PCPDTBT.[11,12] PCPDTBT and PSBTBT have also been used to form the red- to near-infrared-absorbing subcell in state-of-the-art polymer tandem solar cells.[19,20] A major drawback of PCPDTBT in blends with $PC_{70}BM$ is the moderate fill factor (FF), caused by strong non-geminate recombination and a significantly field-dependent generation of free charge-carriers.[21−23] Also, the V_{oc} is only moderate due to the high-lying HOMO level of PCPDTBT. Thus, further improvement of the PCE requires that both the V_{oc} and the FF can be enlarged without deteriorating the favorable optical properties and high internal quantum efficiencies of these polymer blends.

Recently, the V_{oc} of blend devices comprising PCPDTBT or PSBTBT was increased by altering the chemical nature of the electron deficient unit of these DA copolymers. These alterations were motivated by the work of Blouin et al., who showed that replacing the 2,1,3-benzothiadiazole (BT) unit by 2,1,3-benzoxadiazole (BO) simultaneously lowers the HOMO and LUMO energy.[24] Hoven et al. designed a PSBTBO polymer with slightly larger V_{oc} compared to PSBTBT.[25] The overall performance, however, was limited to below 5% due to a lower FF and J_{sc}, and no overall improvement was achieved by replacing the BT with the BO unit. Also Bijleveld et al. synthesized a variety of PCPDT-X polymers.[26] They found a superior performance of PCPDTBO against PCPDTBT due to a higher open V_{oc} and higher FF, resulting in a PCE of 2.5% vs 1.9%, respectively. Again, the J_{sc} and the EQE in the near-IR were lower with BO, and no attempt was made to optimize the blend morphology with solvent additives.

An alternative strategy to improve the V_{oc} is to attach fluorine atoms to the electron-deficient subunits of low-band-gap DA copolymers.[5,27,28] It was shown that this approach simultaneously lowers the HOMO and LUMO level energies, while having no or only minor effect on the optical band-gap.[5,7,29,30] Accordingly, BHJ solar cells comprising these fluorinated copolymers in combination with electron-accepting soluble fullerenes exhibited higher V_{oc} than blends with the corresponding non-fluorinated derivatives.[5,7,27,30−32] Surprisingly, fluorination also improved the J_{sc} values[5,7,30,31,33] and the FFs.[5,7,30−34] These improvements have been explained by high hole mobilities and/or a specific phase-separated morphology of such blends.

In this work, we describe the synthesis and characterization of a novel polymer, poly[2,6-(4,4-bis(2-ethylhexyl)-4*H*-cyclopenta[2,1-b;3,4-b′]dithiophene)-*alt*-4,7-(5-fluoro-2,1,3-benzothiadiazole)] (F-PCPDTBT), formed by the attachment of fluorine to the BT unit of PCPDTBT. Fluorinated benzothiadiazole was first introduced by Li et al. as a new electron-deficient unit in DA copolymers.[33] Due to the strong impact of molecular weight (MW) on solar cell performance,[9,11,12] the polymers PCPDTBT and F-PCPDTBT were synthesized with equivalent MW and compared in blends with $PC_{70}BM$ with regard to solar cell performance and charge-carrier dynamics. Using the techniques of time-delayed collection field (TDCF) and photocharge extraction by linearly increasing voltage (photo-CELIV), conclusive information on the field dependence of charge-carrier generation and non-geminate recombination as well as on transport properties was derived. Plasmon mapping based on energy-filtered transmission electron microscopy (TEM) and ultraviolet photoelectron spectroscopy (UPS) was applied to study the impact of fluorination on the morphology and electronic structure of the blend.

The new polymer F-PCPDTBT shows a lower-lying HOMO level, resulting in a major increase of the V_{oc} to 0.74 V in additive-optimized blends compared to 0.61 V for PCPDTBT. More importantly, the FF and J_{sc} increase from 50% to 59% and from 11.5 to 13.8 mA/cm^2, respectively, which is explained by reduced geminate and non-geminate recombination. In total, fluorination improves the PCE from 3.6% to 6.0% for equivalent MW and preparation conditions. Further optimization of the blend ratio and active layer thickness lead to a PCE of 6.16% for F-PCPDTBT:$PC_{70}BM$ blends. We note that this is below the efficiencies of state-of-the-art single-junction solar cells reported for other polymer:fullerene blends.[6−8,10,35] However, the large V_{oc} in combination with a high quantum efficiency in the near-IR makes F-PCPDTBT extremely attractive for application in polymer tandem solar cells. Published record values for such devices are currently around 8.6%, using the polymer PBDTT-DPP. The extended absorption range and the superior EQE of F-PCPDTBT-based blends compared to the currently best-performing PBDTT-DPP polymer may allow considerable improvement of the overall tandem device performance.[3]

SYNTHESIS

The alternating copolymers poly[2,6-(4,4-bis(2-ethylhexyl)-4*H*-cyclopenta[2,1-b;3,4-b′]dithiophene)-*alt*-4,7-(2,1,3-benzothiadiazole)] (**PCPDTBT**), here referred to as **P−H**) and poly[2,6-(4,4-bis(2-ethylhexyl)-4*H*-cyclopenta[2,1-b;3,4-b′]dithiophene)-*alt*-4,7-(5-fluoro-2,1,3-benzothiadiazole] (**F-PCPDTBT**, here referred to as **P−F**) were synthesized by microwave-assisted Stille cross-coupling polymerization[9] as outlined in Scheme 1. The preparations of the bis-

Scheme 1. Synthesis of PCPDTBT (P−H) from Monomers 1 and 2 and F-PCPDTBT (P−F) from Monomers 1 and 3

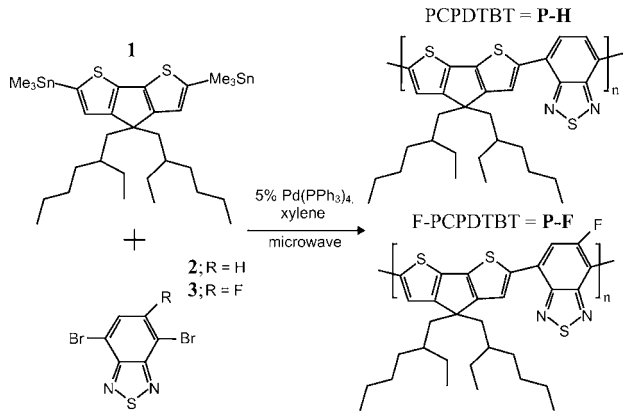

stannylated cyclopentadithiophene[14,36] (**1**) and the 4,7-dibromo-2,1,3-benzothiadiazole[36,37] (**2**) were adapted from literature procedures. The 4,7-dibromo-5-fluoro-2,1,3-benzothiadiazole (**3**) was synthesized starting from 4-fluoro-1,2-phenylenediamine. The ring-closure reaction was done with thionyl chloride, following a bromination with HBr and bromine which is described in the Supporting Information (SI). A stoichiometric ratio of 1:1.15 was applied for the microwave polymerization reaction. The number-average molecular weight (M_n) is around 10 kg/mol with a polydispersity of 2 for both polymers (**P−H** and **P−F**) as determined by high-temperature gel permeation chromatography (GPC) at 135 °C in trichlorobenzene (see Table 1). The attachment of fluorine to the BT unit leads to a more rigid polymer backbone, which reduces its solubility in organic solvents. Differential scanning calorimetry (DSC) measurements did not show any transition peaks for both polymers in temperature range between 0

dx.doi.org/10.1021/ja305039j | J. Am. Chem. Soc. 2012, 134, 14932−14944

Table 1. Characterization of the Polymers P−H and P−F Together with Optical, Transport, and Electronic Properties

	yield [%]	M_n[a] [g/mol]	PDI[b]	λ_{max}[c] [nm]	α_{max}[d] [cm^{-1}]	λ_{onset}[e] [nm]	Eg_{opt}[e] [eV]	IE[f] [eV]	$\mu_{h\ FET}$[g] [$cm^2/(V{\cdot}s)$]	$\mu_{h\ SCLC}$[h] [$cm^2/(V{\cdot}s)$]
P−H	51	10 950	2.09	742	1.67×10^5	855	1.451	5.25	1.4×10^{-3}	1.0×10^{-4}
P−F	67	10 128	2.13	767	1.96×10^5	858	1.446	5.35	1.0×10^{-3}	0.6×10^{-4}

[a]Number-average molecular weight. [b]Polydispersity index. [c]Wavelength of maximum absorption in thin films (see SI). [d]Absorption coefficient deduced from thin-film absorption. [e]Determined by the onset of thin-film absorption, indicated by the arrows in Figure S5. [f]Data obtained from UPS measurements of pure polymer films on PEDOT:PSS substrates. [g]In-plane hole mobility measured with field effect transistors (see SI). [h]Vertical hole mobility deduced from space-charge-limited currents (see SI).

and 270 °C. Thermogravimetric analysis demonstrated high thermal stability of **P−F**, with only 1 wt % loss at 400 °C as shown in the SI.

ELECTRONIC PROPERTIES OF THE POLYMERS IN THE PRISTINE AND BLEND LAYERS

As reported for other DA copolymers, fluorination lowers the polymer ionization energy (IE) in both pristine and blend layers. Figure 1a,b shows the secondary electron cutoff and the

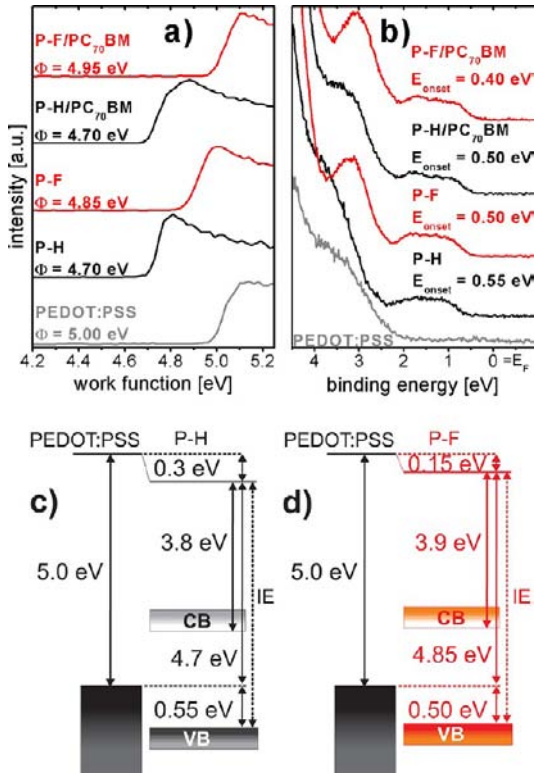

Figure 1. (a,b) Ultraviolet photoelectron spectra of ITO/PEDOT:PSS substrates covered with **P−H** (black) and **P−F** (red) and in additive optimized blends of **P−H**/$PC_{70}BM$ (black) and **P−F**/$PC_{70}BM$ (red): (a) the secondary electron cutoff and (b) the valence band region. Also shown is the energy level alignment diagram (with the IE shown as the dashed line) for ITO/PEDOT:PSS substrates covered with pristine (c) **P−H** and (d) **P−F**.

valence band (VB) region of pristine **P−H** and **P−F** films on PEDOT:PSS and of polymer/$PC_{70}BM$ blends processed with 3% diiodooctane (DIO) for **P−H** and 1% DIO for **P−F** (these concentrations were found to give optimum solar cell performance as outlined in detail below). The work function (Φ) of the PEDOT:PSS layer was 5.0 eV. Compared to the PEDOT:PSS covered substrate, Φ for the polymer-coated samples is smaller by 0.30 (**P−H**) and 0.15 eV (**P−F**). From the pristine polymer spectra the VB onset was found at 0.55 and 0.50 eV below the substrate Fermi energy (E_F) for **P−H** and **P−F**, respectively. Combining these data results in an IE of 5.25 eV for **P−H** and 5.35 eV for **P−F**, meaning that the position of the VB onset is 0.1 eV deeper with fluorination (see Figure 1c,d for the respective energy schemes). The position of the conduction band (CB) onset is estimated by setting the energetic difference between the CB and the VB onsets to the optical band-gab Eg_{opt} (see Table 1). Similar values for the IE compared to the pristine polymer films are obtained for polymer/$PC_{70}BM$ blend films ($IE_{P-H(blend)}$ = 5.20 eV and $IE_{P-F(blend)}$ = 5.35 eV). Assuming that there is no surface dipole layer formation between the polymer and the fullerene-rich domains, **P−F** has a 0.1 eV larger energetic offset between the VB onset of the polymer and the LUMO of $PC_{70}BM$ compared to **P−H**. Note that the UPS spectra of the blend films in the low binding energy region are dominated by features from the polymer, and no features attributed to the molecular levels of $PC_{70}BM$ are observed. We conclude that the topmost layer of the blend films consists only of the pristine polymers.

OPTICAL PROPERTIES OF PRISTINE POLYMER AND BLEND LAYERS

Non-normalized absorption spectra of **P−H**/$PC_{70}BM$ and **P−F**/$PC_{70}BM$ blend films with a thickness of 100 nm processed with different amounts of DIO are displayed in Figure 2. As has

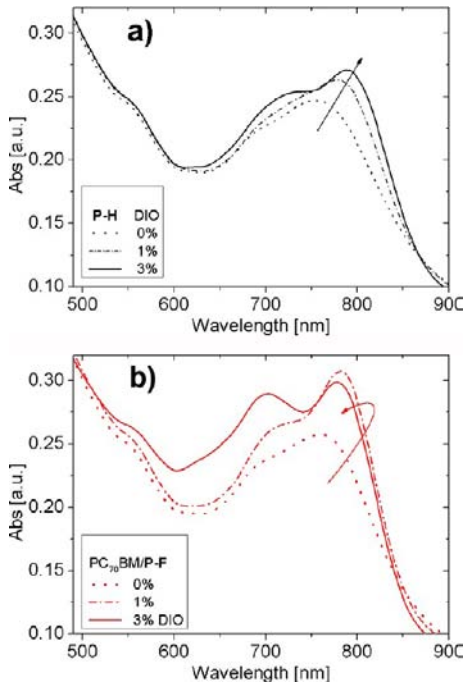

Figure 2. Absorption spectra (not normalized) from 100 nm thick films of polymers **P−H** (a) and **P−F** (b) blended with $PC_{70}BM$ in a 1:3 weight ratio processed without DIO (dots), with 1% DIO (dashed lines), and with 3% DIO (solid lines).

dx.doi.org/10.1021/ja305039j | J. Am. Chem. Soc. 2012, 134, 14932−14944

been reported before, adding DIO to **P−H**/$PC_{70}BM$ continuously increases the strength of the low-energy polymer absorption centered around 800 nm, which is explained by a higher degree of intra- and interchain ordering.[38] Recent in situ X-ray studies revealed that the solvent additive promotes the formation of polymer crystallites during prolonged film drying.[39] These effects are more pronounced for the **P−F**-based blends, with the long-wavelength peak dominating the spectra already at a DIO concentration of 1%, indicating a high tendency of the **P−F** chains to aggregate even in presence of $PC_{70}BM$. A higher tendency for chain aggregation is indicated in absorption spectra taken on the pristine polymers in solution and solid states, as shown in Figure S5 in the SI. Son et al. reported improved intermolecular order in pristine layers of fluorinated polythienothiophene-*co*-benzodithiophenes (PTBs).[32] It was proposed that the fluorinated polymers exhibit a more planar backbone conformation, allowing for a more regular packing in the solid state. The authors further suggested that intermolecular interaction might be enhanced upon F-attachment via the interaction of fluorinated electron-deficient units and electron-rich aromatic rings. Strong intermolecular interaction was proposed by Li et al. to cause a reduced stacking distance in pristine layers of fluorinated BDT:BT copolymers.[33] We also note the overall higher absorbance of blends with **P−F** for comparable thickness and processing conditions, which is particularly evident in the wavelength range dominated by the polymer. As this effect is seen also in the solution- and solid-state spectra of the pristine layers, we explain this feature on the basis of the higher absorption cross section of the fluorinated chains. Higher absorption coefficients of fluorinated DA copolymers in solution or solid state have been shown by others,[7,31] but a conclusive explanation for this enhancement is still missing. Peak positions and absorption coefficients for the pristine and the blend layers are summarized in Tables 1 and 2. As a combined effect of a higher absorption cross section and improved aggregation, blends comprising F-PCPDTBT exhibit higher solid-state absorption coefficients, especially in the red part of the spectrum. Note that the optical band-gap of the solid pristine polymers (determined by extrapolation of the linear decay of absorption around 810 nm to zero absorbance as indicated by the arrows in Figure S5) is almost unchanged upon fluorination, despite a 0.1 eV increase of the IE upon fluorination. This is in accordance with previous reports on other fluorinated DA copolymers.[5,7,33]

Table 2. Optical Characterization of Polymers P−H and P−F Blended with $PC_{70}BM$, Processed with Different Amounts of Additive

	DIO [%]	$\lambda_{max,1}$ [nm]	$\alpha_{max,1}$ [10^4 cm^{-1}]	$\lambda_{max,2}$[a] [nm]	$\alpha_{max,2}$[a] [$10^4 cm^{-1}$]
P−H	0	754	5.69	692	5.14
P−H	1	777	6.06	696	5.41
P−H	3	788	6.24	730	5.84
P−F	0	758	5.93	692	5.38
P−F	1	782	7.01	709	6.04
P−F	3	777	6.87	702	6.66

[a]This spectral feature appears as a shoulder in the spectra of the layers processed without DIO.

MORPHOLOGICAL PROPERTIES OF THE BLEND LAYERS

To analyze the effect of fluorination on the morphology of blends layers with $PC_{70}BM$, we performed plasmon mapping based on energy-filtered TEM.[40,41] For blends of materials with low degree of crystallinity, conventional TEM relies mainly on the mass density contrast. In contrast, the method employed here makes use of the different characteristic plasmon energies of the two active blend components to identify polymer- and fullerene-rich domains with high spatial resolution. Figure 3 shows the corresponding plasmon maps for both PCPDTBT and F-PCPDTBT-based blends processed with different amounts of DIO. These figures plot the energy of the maximum plasmon absorption for each lateral coordinate. Reference measurements on pristine layers showed that the energy of maximum plasmon absorption is 25.1 eV for pure $PC_{70}BM$, 22.4 eV for the pure **P−H**,[22] and 22.2 eV for **P−F**. Thus, the black areas in Figure 3 refer to $PC_{70}BM$-rich domains. For both **P−H** and **P−F**, the images show that the phase separation coarsens with increasing amount of the additive, which is in agreement with earlier studies on **P−H**-based blends using conventional TEM under defocusing conditions.[12,18]

To quantify the structural heterogeneity of the blends, the plasmon maps have been analyzed with regard to the mean areas of domains that are polymer- and PCBM-rich (with respect to the composition of a homogeneous 1:3 mixture of both components). These values are plotted in Table 3. Details of the analysis and histograms showing the number of pixels with a certain plasmon energy can be found in the SI. These data prove consistently that fluorination enforces the formation of more extended and purer polymer-rich phases. We attribute this to the stronger tendency of the F-PCPDTBT to aggregate, as outlined above. Noticeably, only 1% of DIO needs to be added to the **P−F**-based blend to induce a polymer-rich domain area as large as that in the optimized **P−H** blend processed with 3% DIO. Fluorination also affects the size and purity of the fullerene-rich domains, though this effect becomes less pronounced with increasing DIO concentration. Mean areas of the polymer and fullerene-rich domains are largest for the **P−F** blend processed with 3% DIO. It has been pointed out by Son et al. that fluorination of the donor polymer introduces fluorophobility for PCBM, enforcing phase separation between the donor and acceptor components in the blend layer.[32] Improved phase separation into purer and larger domains was also reported for blends of other fluorinated DA copolymers with PCBM.[30,33,34] Note that the domain areas listed in Table 3 have been deduced from TEM images which constitute 2D projections of the true 3D bulk morphology. Therefore, the analysis of such pictures underestimates the true domain area. In fact, PCPDTBT crystal sizes larger than 10 nm have been reported in DIO-processed **P−H** blends.[42,43]

BHJ SOLAR CELL CHARACTERISTICS

Figure 4a shows the steady-state solar cell characteristics measured under simulated AM 1.5G with 100 mW/cm^2 for the two polymers blended with $PC_{70}BM$ and processed with different amounts of DIO. The corresponding performance data are listed in Table 4. Values for **P−H**-based blends are lower than state-of-the-art reports with high-molecular-weight polymers[11,12,18] but compare well to efficiencies for blends with PCPDTBT of similar MW.[9] Upon fluorination V_{oc} is increased

dx.doi.org/10.1021/ja305039j | J. Am. Chem. Soc. 2012, 134, 14932−14944

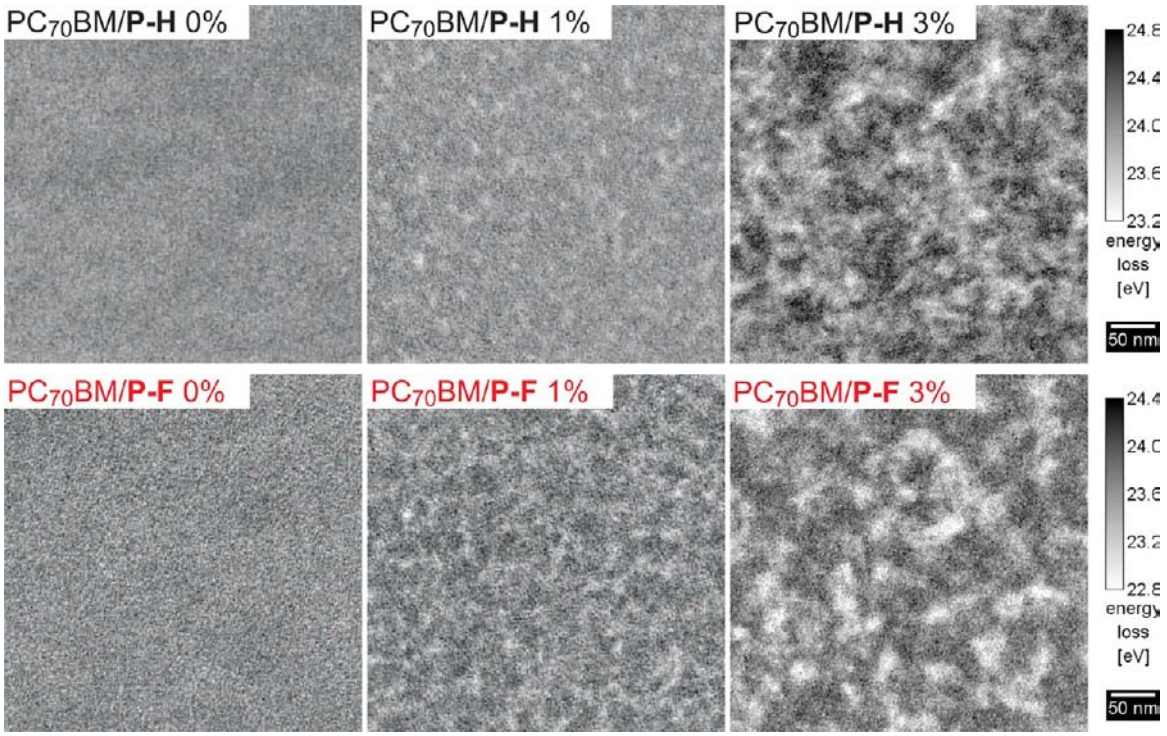

Figure 3. Plasmon mapping based on energy-filtered TEM of films made from blends of **P−H** (upper panel) and **P−F** (lower panel) with $PC_{70}BM$ at a 1:3 weight ratio and processed with different concentrations of DIO. The amount of DIO was 0, 1, and 3% for the images displayed in the left, middle, and right columns, respectively. The scale bar is the energy of maximum plasmon absorption (energy loss), where dark areas refer to $PC_{70}BM$-rich phases (see text and SI).

Table 3. Mean Area of the Domains Assigned to the Polymer- or PCBM-Rich Phase for P−H and P−F Blended with $PC_{70}BM$, Processed with Different Amounts of Additive

		domain area[a] [nm^2]	
	DIO [%]	polymer	$PC_{70}BM$
P−H	0	5[b]	9.9
P−H	1	8.4	21
P−H	3	13.9	47
P−F	0	11.5	16.2
P−F	1	14.7	28.3
P−F	3	18.2	50

[a]See SI for the details on the calculation of the domain area. [b]A domain area of 5 nm^2 is close to the size of one pixel (2 nm^2) in the plamon maps, meaning that within the resolution of the experiment the **P−H**:$PC_{70}BM$ blend processed without DIO is a homogeneous mixture of the two components.

by ∼130 mV. Within the accuracy of the UPS measurement, the increase in V_{oc} corresponds well to the increase in polymer IE upon fluorine attachment, which is 100 meV for the pristine layer and 150 meV for the blend.

In accordance with the absorption and TEM data, the optimum amount of processing additive is reduced from 3% to 1% due to the stronger tendency of **P−F** to aggregate. Importantly, also the J_{sc} of the additive-optimized blend with **P−F** is significantly higher (13.8 mA/cm^2 for **P−F** with 1% DIO compared to 11.46 mA/cm^2 for **P−H** with 3% DIO). This higher current can be related to an enlarged EQE throughout the entire absorption range as shown in Figure 4b, approaching values of 50% between 400−500 and 700−800 nm. Note that the mean EQE of our optimized **P−F** blend is 10% larger compared to that of the optimized blend with **P−H** of almost

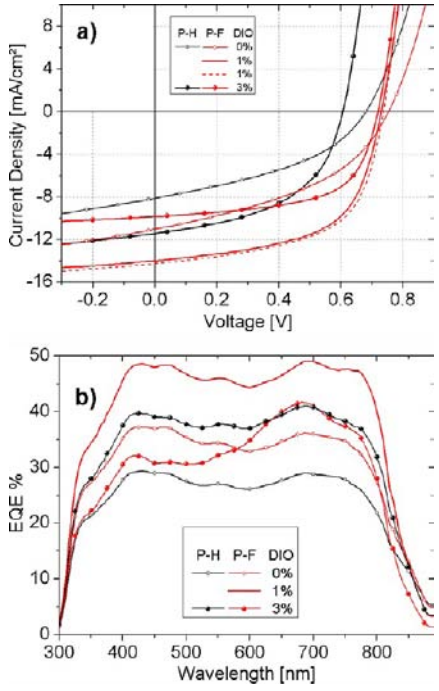

Figure 4. (a) Solar cell characteristics measured under simulated AM 1.5G irradiation with 100 mW/cm^2 (corrected for spectral mismatch) for 100 nm thick blends of **P−H** (black) and **P−F** (red) with $PC_{70}BM$ (1:3 ratio), processed without DIO (lines + open circles), with 1% DIO (solid lines), and with 3% DIO (lines + filled circles). The dashed line shows data for a **P−F**:$PC_{70}BM$ blend with an optimized blend ratio of 1:2.5, a DIO concentration of 1%, and a ca. 90 nm active layer thickness. (b) Corresponding external quantum efficiency spectra.

dx.doi.org/10.1021/ja305039j | J. Am. Chem. Soc. 2012, 134, 14932−14944

Table 4. Photovoltaic Properties and Characteristic Parameters Describing the Generation, Transport, and Recombination of the Polymers P−H and P−F in 1:3 Blends with $PC_{70}BM$

	DIO [%]	J_{sc}[a] [mA/cm^2]	V_{oc}[a] [mV]	FF[a] [%]	PCE[a] [%]
P−H	0	8.05	677	40.3	2.20
P−H	1	10.39	640	46.5	3.09
P−H	3	11.46	610	50.3	3.51 (3.59)
P−F	0	11.01	751	41.2	3.40
P−F	1	13.83	731	58.6 (59.6)	5.92 (5.98)
P−F[b]	1	14.08	740	58.0	6.04 (6.16)
P−F	3	9.85	722	60.3	4.28

[a]Data have been averaged over 6 devices; the performance of the best device is given in parentheses. Standard deviation of PCE was less than 0.06. [b]Optimized device with a blend ratio of 1:2.5 and an active layer thickness of ∼90 nm.

identical MW and still 5% larger than the mean EQE measured on blends with higher-MW **P−H**.[44] Optical simulations with a transfer matrix formalism (not shown here) revealed that the higher absorption coefficients of the fluorinated blends raise the fraction of photons absorbed in the active layer only slightly, meaning that fluorination must also increase the efficiency of converting an absorbed photon into an extracted carrier. As outlined in the Introduction, higher J_{sc} values and EQEs have occasionally been reported for blends of other fluorinated DA copolymers with PCBM.[5,7,30,31,33]

In addition to a higher J_{sc} and EQE, the fluorination increases the FF by almost 10% in additive optimized solar cells with the same MW. The FFs of all our **P−F**-based DIO processed blends actually exceed the highest value (55%) ever reported for high-MW PCPDTBT.[11]

A further improvement of the **P−F**:$PC_{70}BM$ blend performance was achieved by slightly decreasing the active layer thickness[44] and by using a 1:2.5 (instead of 1:3) blend ratio, allowing the blend to absorb more strongly in the red to infrared part of the spectrum. We note that FF is not significantly altered when the blend ratio is varied between 1:3 and 1:2.5. Thus, we presume that the charge-carrier dynamics is only weakly affected by the small change in blend ratio. These optimized blends exhibited PCEs of up to 6.16% (6.04% on average), meaning that **P−F** outperforms high-molecular-weight PCPDTBT[11,12] and PSBTBT.[16,45]

CHARGE-CARRIER GENERATION AND RECOMBINATION

To shed some light on the fundamental processes causing the observed increase in J_{sc} and FF upon fluorination, we studied the efficiency for free-carrier formation and recombination using TDCF measurements.[46] The measurement scheme is outlined in the SI. With TDCF, charges are generated with a nanosecond laser pulse at voltages (pre-bias, V_{pre}) typical for solar cell operation. After a defined delay time a high constant reverse bias (collection bias, V_{coll}) is applied to extract all laser-generated charges which did not undergo recombination or which had not been extracted during the delay. Performing experiments with different pre-bias and delay time allows us to assess both the efficiency of free-carrier formation and non-geminate recombination as functions of bias.[22,46]

Field Dependence of Free-Carrier Generation. To address the effect of electric field on the generation of free carriers from the splitting of bound polaron pairs (PPs), TDCF experiments must be conducted under conditions where significant non-geminate recombination losses during delay and extraction are absent. It was shown before that free-carrier generation from either hot excitons or bound PPs in PCPDTBT is fully completed within a few nanoseconds after pulsed illumination.[47−50] Our previous TDCF studies on high-molecular-weight PCPDTBT showed that non-geminate recombination is insignificant within the first few tens of nanoseconds after excitation at moderate pulse fluences.[22] This was also proven by the linear dependence of the extracted charge on pulse fluence when setting the delay to 10 ns.[22] In this linear range the pulse fluence can be adjusted to create charge-carrier densities being comparable to 1 sun steady-state conditions.[51] Performing TDCF measurements in this range with different pre-bias and a short delay time between laser pulse and extraction, therefore, allows us to directly address the field dependence of free charge-carrier generation.

Figure 5a shows the total extracted charge Q_{tot} (being the integral over the whole current transient) versus applied bias during generation for a delay time of 10 ns. As non-geminate recombination is insignificant under these conditions, Q_{tot} is a direct measure of the free charge generated by the laser pulse at a given bias in competition with geminate recombination. By normalizing the generated charge to the respective value at the

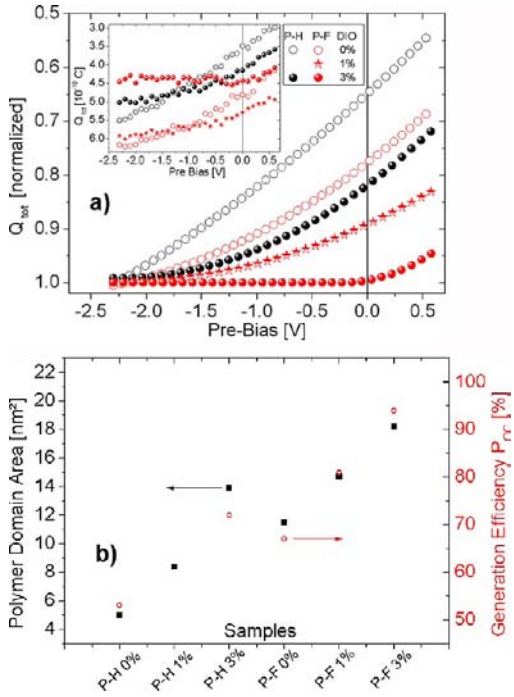

Figure 5. (a) Total extracted charge Q_{tot} deduced from TDCF measurements with 10 ns delay and 0.25 μJ/cm^2 pulse fluence as a function of pre-bias. Blends with **P−H** (black) and with **P−F** (red) are plotted for different amounts of additive: without DIO (open circles), with 1% DIO (stars), and with 3% DIO (filled circles). Values have been smoothed and normalized to the generated charge at the highest accessible bias of −2.3 V. The *y*-axis is scaled downward for better comparison with the negative photocurrent. The inset shows the raw, non-normalized data. (b) Comparison of the mean polymer domain size deduced from the plasmon maps in Figure 3 (left scale, black) with the relative generation efficiency P_{oc} at open-circuit conditions (right scale, red), being defined as the ratio of generated charges at open circuit compared to −2.3 V (see Table 5).

dx.doi.org/10.1021/ja305039j | J. Am. Chem. Soc. 2012, 134, 14932−14944

Table 5. Characteristic Parameters Describing the Generation, Transport, and Recombination of the Polymers P−H and P−F in 1:3 Blends with $PC_{70}BM$

	DIO [%]	P_{oc} [a] [%]	γ_{sc} [b] [10^{-17} m^3/s]	γ_{oc} [b] [10^{-17} m^3/s]	μ_e [c] [10^{-4} $cm^2/(V\cdot s)$]	ζ [d]
P−H	0	53	2.9	6.5	2.3	0.2
P−H	3	72	2.5	8.0	6.0	0.07
P−F	0	67	1.2	1.7	1.2	0.14
P−F	1	81	1.1	2.4	4.2	0.04
P−F	3	94	1.2	2.6	5.7	0.03

[a]The relative dissociation probability, P_{oc}, is the amount of generated charges close to V_{oc} relative to the charge generated at −2.3 V. [b]Bimolecular recombination coefficients γ_{SC} and γ_{oc} at short and open circuit, respectively. [c]Mobility deduced from photo-CELIV at a field strength of 200 $V^{1/2}\cdot cm^{-1/2}$. [d]Langevin reduction factor ζ estimated from the measured mobility at a field strength of 175 $V^{1/2}\cdot cm^{-1/2}$;

highest reverse bias of −2.3 V, the field dependence of free charge-carrier generation, i.e., the variation of Q_{tot} with pre-bias, can be compared for different blends. In great contrast to the well-known P3HT:PCBM system showing no field dependence of free charge generation,[46] the performances of all blends studied here are strongly limited by the field-dependent splitting of bound PPs.

For blends of **P−H** with $PC_{70}BM$ processed without DIO, we find that the efficiency for free-carrier generation at open-circuit conditions relative to the efficiency at −2.3 V, P_{oc}, to be only 53% (Table 5), suggesting efficient geminate recombination. Processing with 3% DIO increases P_{oc} to ca. 72%, implying a geminate loss of about 30%. These numbers compare very well to geminate losses at zero field determined by TAS. For example, Laquai and co-workers determined the total loss due to geminate recombination to about 50% in samples prepared without ODT and 30% in samples prepared with ODT.[49] More recently, Yamamoto and co-workers estimated the geminate loss in blends of PCPDTBT and $PC_{70}BM$ processed with 2% DIO to be 30%.[50]

Importantly, the field dependence of free charge generation becomes considerably weaker upon fluorination, which is clearly evident when comparing blends with **P−H** and **P−F** processed with the same amount of DIO. Also, processing with DIO weakens this field dependence, as shown earlier for non-fluorinated PCPDTBT.[22] The good correlation between P_{oc} and the mean polymer domain area in Figure 5b, and the distinct changes of the optical absorption properties of the blends upon processing with DIO and/or fluorination, suggest that a weaker field dependence of free-carrier generation is caused by the formation of larger (and probably purer) domains with better interchain order. Noticeably, blends with **P−F** processed with 3% DIO, whose morphology is characterized by rather pure polymer domains with the maximum domain size in lateral dimension, show only a 5% loss of efficiency for free charge-carrier formation when approaching V_{oc}.

The inset of Figure 5a shows the non-normalized raw data for the extracted free charge as a function of pre-bias. Note that the excitation was at a wavelength of 500 nm, where all studied blend layers exhibit nearly the same absorption (see Figure 2). Apparently, additive-optimized blends with **P−F** generate ∼20% more free charges than their **P−H** counterparts over the entire bias range studied here for a comparable number of absorbed photons, meaning that exciton migration to the bulk heterojunction and/or free-carrier formation in competition with geminate recombination must be more efficient when using fluorinated donor polymers. As a similar enhancement is seen for the two blends processed without DIO where the donor and acceptor components are well intermixed, we presume that the fluorination promotes free-carrier formation via more efficient dissociation of bound PPs. Recently, a correlation has been established between the efficiency for free-carrier formation and the charge-transfer characteristics of DA polymers.[52] It was shown that fluorination increases the difference between the ground- and excited-state dipole moment $\Delta\mu_{ge}$ for PTB polymers, indicating enhanced charge transfer during excitation, which in turn shall facilitate the formation of free charges.[52] We propose that a similar mechanism causes the efficient formation of free charges in the fluorinated PCPDTBT as measured with TDCF.

Although blends with **P−F** processed with 3% DIO display the weakest field dependence of free-carrier formation, this blend shows an overall low efficiency for free-carrier generation at 500 nm. We attribute this to the presence of large and rather pure domains, implying a low probability for excitons generated on either the polymer or the $PC_{70}BM$ to reach the heterojunction. Note that the EQE in these blends is reduced mainly in the wavelength range where the $PC_{70}BM$ absorption is dominant, consistent with the appearance of large fullerene clusters in the plasmon maps in Figure 3, as discussed above.

Non-geminate Recombination. It was recently shown that the performance of blends of PCPDTBT with $PC_{70}BM$ is severely limited by efficient non-geminate recombination within the solar cell working regime, even in additive-optimized blends.[21,22] To assess the efficiency and kinetics of non-geminate recombination, we performed TDCF measurements with variable delay time between the laser pulse and the collection voltage. Figure 6 shows the results for **P−H**- and **P−F**-based additive optimized blends with a pre-bias setting close to the respective V_{oc}. Here, Q_{pre} is the charge extracted during delay. At conditions close to V_{oc} the drift of the photogenerated

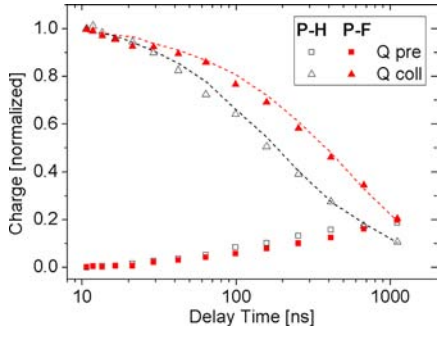

Figure 6. Precharge Q_{pre} and collected charge Q_{coll} derived from TDCF transients with different delay times and pre-bias setting close to V_{oc} (V_{pre} = 0.6 V for **P−H** and 0.7 V for **P−F**). The dashed lines are the corresponding BMR fits. Data are normalized to the initially photogenerated charge for better comparison.

dx.doi.org/10.1021/ja305039j | J. Am. Chem. Soc. 2012, 134, 14932−14944

charge-carriers is very slow, and Q_{pre} increases only gradually with time. Q_{coll} is the charge collected after a defined delay time by application of the collection bias, i.e., the charge which has not been extracted and which did not undergo non-geminate recombination during delay.[46] With increased delay time, more and more charges recombine non-geminately, leaving less charge available for extraction. Obviously, more charge can be collected for blends with **P−F** at a specific delay time, meaning that non-geminate recombination of charges must be reduced.

Fits to the experimental data with an iterative routine according to eq S1 (see SI) are represented by the dashed lines in Figure 6. The decay of Q_{coll} with delay time can be well described by second-order bimolecular recombination (BMR) with γ_{BMR} being the bimolecular recombination coefficient. The agreement between the experimental data and the fit is very good, considering that γ_{BMR} is the only adjustable parameter. Values for γ_{BMR} at different pre-bias are plotted in Figure 7. The

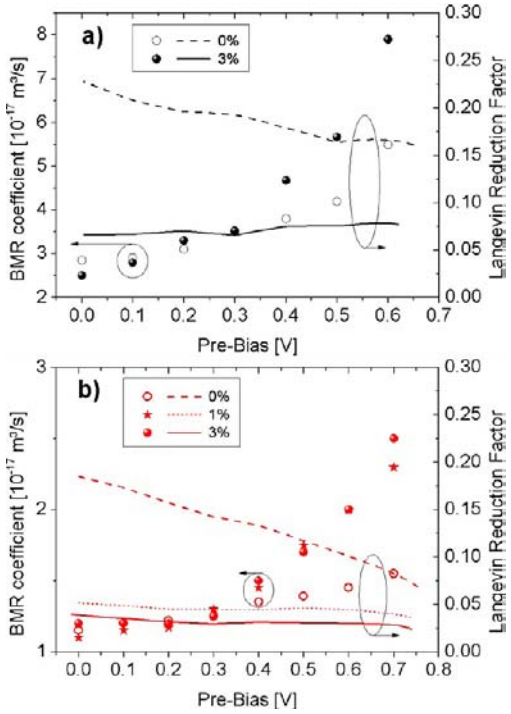

Figure 7. Left scale: Bimolecular recombination coefficient γ_{BMR} as a function of pre-bias deduced from fits (using eq S1) to the decay of the collected charge as shown in Figure S8. (a) Blends containing **P−H** (black) without additive (open circles) and with 3% DIO (filled circles). (b) Blends containing **P−F** (red) without additive (open circles), with 1% DIO (stars), and with 3% DIO (circles) Right scale: Langevin reduction factor obtained from the measured mobility and its field dependence for (a) **P−H**-based blends (black) processed without DIO (dashed line) or with 3% DIO (solid line) and (b) **P−F**-based blends (red) processed without DIO (red dashed line), with 1% DIO (red dotted line), and with 3% DIO (red solid line).

BMR coefficients of all blends are rather high, ranging between 1×10^{-17} and 8×10^{-17} m^3/s. These values are considerably larger than those reported for annealed blends of P3HT and PCBM, which are typically of the order of 10^{-18} m^3/s, meaning that non-geminated recombination is efficient in all of our blends. Our values for **P−H** blends at V_{oc} agree very well with zero-field BMR coefficients (measured with TAS at moderate carrier densities) in PCPDTBT:$PC_{61}BM$ blends processed without (3.2×10^{-17} m^3/s) or with (6.3×10^{-17} m^3/s) ODT as determined by Etzold et al.,[49] and they show reasonable agreement with $\gamma_{BMR} = 10 \times 10^{-17}$ m^3/s measured for a PCPDTBT:$PC_{70}BM$ blend processed with DIO by Yamamoto et al.[50] Noticeably, fluorination consistently reduces γ_{BMR} by a factor of 2−3 for blends processed either with or without DIO (see also Table 2). As outlined below, this reduction is a consequence of a smaller mobility in combination with a lowering of the Langevin reduction factor.

Figure 7 also shows that γ_{BMR} increases with increasing bias (decreasing internal electric field) for all measured blends, meaning that the coefficient is largest near open-circuit conditions. A proncounced increase of γ_{BMR} with decreasing field has recently been reported for higher-molecular-weight PCPDTBT.[22] This behavior was attributed to a pronounced negative field dependence of the charge-carrier mobility in the blend layers. Koster pointed out that a negative field dependence of mobility is generally expected for phase-separated blends of materials with distinctly different HOMO and LUMO energies.[53] In such blends, charges moving, e.g., in the donor phase occasionally need to perform jumps against the electric field direction to circumvent domains formed by the acceptor. Increasing the electric field reduces the rate for these back-jumps, decreasing the overall mobility of charge-carriers.

Figure 8 shows mobilities deduced from photo-CELIV measurements with variable voltage slopes in the low-field regime (below 300 $V^{1/2}$ $cm^{-1/2}$) following the analysis proposed by Bange et al.,[54] and mobilities at higher electric fields derived from TDCF measurements by extrapolating the initial photocurrent slope to zero[46] as outlined in the SI. In the

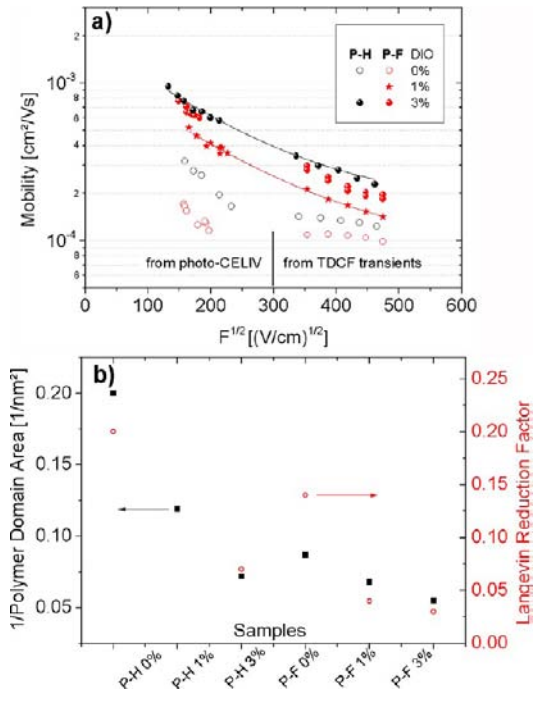

Figure 8. (a) Field-dependent mobilities measured with photo-CELIV (values in the field range below 300 $V^{1/2}$ $cm^{-1/2}$) and TDCF (values in the field range above 300 $V^{1/2}$ $cm^{-1/2}$) for blends with **P−H** (black) and **P−F** (red), without additive (open circles), with 1% DIO (stars), and with 3% DIO (circles). The lines are guides to the eyes for the additive optimized blends. (b) Comparison of the inverse mean polymer domain area (left scale, black) deduced from plasmon maps with the Langevin reduction factor (right scale, red) as shown in Table 5.

dx.doi.org/10.1021/ja305039j | J. Am. Chem. Soc. 2012, 134, 14932−14944

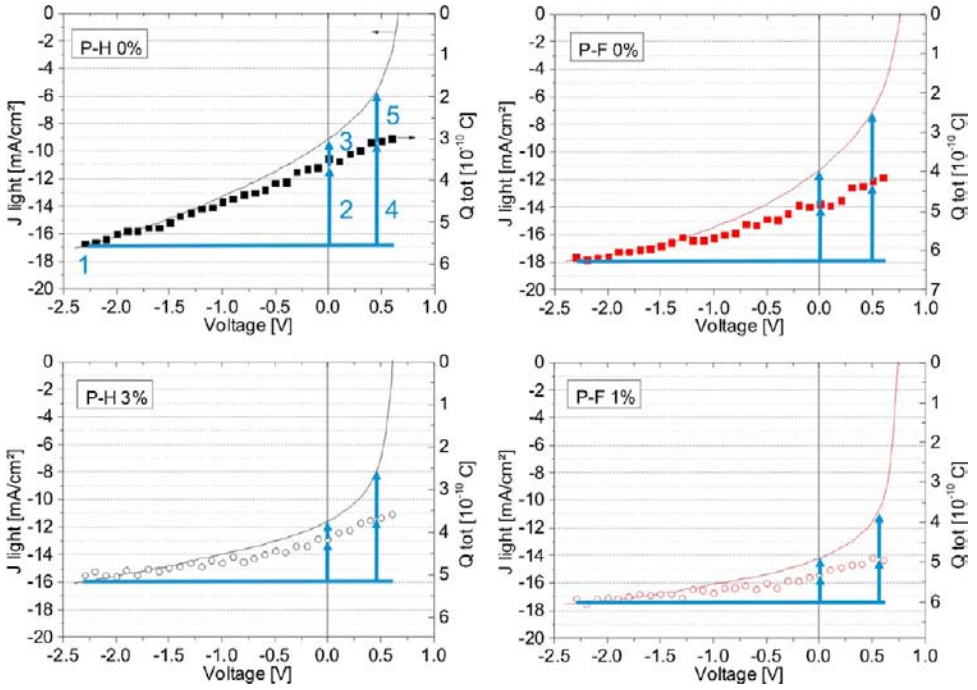

Figure 9. Measured $J-V$ characteristics under simulated AM 1.5G illumination, J_{light} (left scale) compared to the total charge Q_{tot} measured by TDCF at different pre-bias (right scale), for blends containing **P−H** (left) or **P−F** (right). Devices were processed either without (upper row) or with the optimum concentration of the solvent additive DIO (lower row). Q_{tot} is scaled to match the current under illumination at a bias of −2.3 V. Arrows show geminate and non-geminate losses at short circuit and the maximum power point (see Table 6 for the assignment of the arrows and the corresponding loss currents).

latter case, the extraction bias was varied between 0.5 and 1.5 V to ensure that the decay is not determined by recombination (as for lower fields) and not limited by the RC time (as for higher fields). It was reported earlier that electrons are the faster charge-carriers in PCPDTBT:PCBM blends.[23] Therefore, we attribute the mobility determined by photo-CELIV and TDCF to the electrons. We find that the processing additive increases the electron mobility by a factor of 3−4 for blends with either **P−H** or **P−F**, which is in accordance with earlier measurements on PCPDTBT.[22,55]

Interestingly, we measured lower mobilities for blends of the fluorinated donor polymer processed without DIO. Presuming that we record electron mobilities in all cases, this observation is rather surprising at first glance. However, attachment of the electron-withdrawing fluorine might lead to higher local dipole moments along conjugated polymer segments, resulting in a broadening of the density of states in both the electron- and the hole-transporting phases for highly intermixed blends.[56] In accordance with this interpretation, we find that fluorination reduces both the lateral and vertical hole mobility in pristine PCPDTBT layers, despite better chain packing (see SI). Also, increasing the domain size upon processing with DIO caused the mobility of the **P−F**-based blend to approach the value measured on the non-fluorinated system (see also the 3% DIO data in Table 2). In these blends with well-separated domains, electrons will move a greater distance to the donor-phase, which will diminish the possible distortion of electron transport by molecular dipoles located in the polymer phase.

Knowing the field dependence of γ_{BMR} and the carrier mobility in the same layer allows us to compare the BMR coefficient in the different blends with the Langevin recombination coefficient for three-dimensional recombination in an homogeneous medium, $\gamma_L(F) = e[\mu_e(F) + \mu_h(F)]/\varepsilon_o\varepsilon_r$. Here μ_e and μ_h are the mobility of electrons and holes, respectively, e the elementary charge, and F the internal electric field.[22] Blends of conjugated polymers and fullerene often reveal a reduced BMR recombination, as expressed by a Langevin reduction factor $\zeta(F) = \gamma_{BMR}(F)/\gamma_L(F)$ smaller than 1.[57,58] Experimental and theoretical work suggested that phase separation of the donor and acceptor components in pure domains suppresses recombination.[22,59−64] Figure 7 plots $\zeta(F)$ for all blends studied. In calculating $\gamma_L(F)$, we assumed that μ_h is 2 times smaller than μ_e over the entire field range, as shown earlier for high-molecular-weight PCPDTBT.[22] We find that $\zeta(F)$ is nearly independent of the internal electric field F (except for the F-PCPDTBT blend processed without DIO), meaning that the negative field dependence of γ_{BMR} reported above is mainly caused by a decrease of carrier mobility with increasing field. Second and more important, we consistently observe lower values of $\zeta(F)$ for blends containing **P−F**, and $\zeta(F)$ is further lowered upon processing with the additive.

Figure 8b plots the Langevin reduction factor near V_{oc} for the different blends together with the inverse of the average polymer domain area. Clearly, fluorination reduces the rate at which free carriers recombine. The apparent anti-correlation between the polymer domain size and ζ suggests that this reduction is related to the presence of larger and purer domains in blends with **P−F**. For example, ζ of the **P−F**-containing blend processed with 3% DIO, which has the largest mean area of the polymer-rich domains, is only 0.03, meaning that non-geminate recombination in this blend is significantly suppressed compared to the Langevin limit.

dx.doi.org/10.1021/ja305039j | J. Am. Chem. Soc. 2012, 134, 14932−14944

Table 6. Geminate (GEM) and Non-geminate (NG) Loss Currents in 1:3 Blends of P−H or P−F with $PC_{70}BM$, Processed with Different Amounts of DIO

	DIO [%]	1 $J_{gen}(-2.3\ V)$ [mA/cm^2]	2[a] $J_{GEM}(SC)$ [mA/cm^2]	3[a] $J_{NG}(SC)$ [mA/cm^2]	4[a] $J_{GEM}(MPP)$ [mA/cm^2]	5[a] J_{NG} (MPP) [mA/cm^2]	MPP [V]
P−H	0	16.74	5.74	1.88	7.39	3.62	0.45
P−H	3	15.93	3.19	1.14	4.48	3.27	0.46
P−F	0	17.81	4.13	2.45	5.70	4.97	0.50
P−F	1	17.48	2.22	1.08	3.16	3.49	0.56

[a]Loss currents 2−5 are described in text and shown by the arrows in Figure 9.

DISCUSSION

The knowledge of the field dependence of free-carrier generation allows us to assess the geminate and non-geminate losses that limit the device performance of our blends.

For this, we express the current flowing through the device under illumination $J_{light}(V)$ in terms of current densities describing the generation and non-geminate loss of free charge carriers in the active layer per unit area:

$$J_{light}(V) = J_{gen}(V) - J_{NG}(V) \quad (1)$$

Here, J_{gen} is the generation current density (the generated free charge per unit area and time) and J_{NG} the loss current density including non-geminate recombination and diffusion to the wrong contact. Figure 9 plots the bias-dependent light current $J_{light}(V)$ together with $Q_{tot}(V)$, the latter being a direct measure for the efficiency of free-carrier generation at the given voltage.

For all blends, the course of the current−voltage characteristics $J_{light}(V)$ at sufficiently negative reverse bias follows $Q_{tot}(V)$, meaning that non-geminate recombination losses are negligible at these conditions and that the field-dependent free-carrier generation rate determines J_{light} under simulated AM 1.5G illumination. Therefore, $Q_{tot}(V)$ can be translated into $J_{gen}(V)$ via

$$J_{gen}(V) = J_{gen}(-2.3\ V)\frac{Q_{tot}(V)}{Q_{tot}(-2.3\ V)} \quad (2)$$

Clearly, $J_{gen}(V)$ is smaller than $J_{gen}(-2.3\ V)$ under solar cell working conditions, meaning that geminate recombination of bound polaron pairs competes with their dissociation into free charges in the corresponding voltage regime. This loss can be approximated by $J_{GEM}(V) = J_{gen}(-2.3\ V) - J_{gen}(V)$. As most J−V characteristics do not saturate at reverse bias, we presume that geminate recombination is still active at −2.3 V, meaning that the given $J_{GEM}(V)$ are minimum values for the total geminate loss.

Table 6 summarizes J_{GEM} and J_{NG} at short-circuit conditions (SC) and at the maximum power point (MPP), respectively. These losses are also indicated by arrows in Figure 9. For the **P−H** blend processed without DIO, geminate recombination losses are severe. Geminate recombination reduces the photoinduced current density by at least 34% at SC, and this loss increases further to 44% at the MPP. The progressive increase in J_{GEM} with increased bias is a major cause for the low FF of this device. Geminate recombination losses are reduced by processing with DIO and fluorination of the donor polymer. For the optimized **P−F** blend, geminate recombination losses are only 13% at SC, increasing slightly to 18% when going to the MPP. These numbers are significantly smaller than the corresponding values (20% and 28%) for the optimized **P−H** blend.

Regarding non-geminate losses in devices processed without DIO, $J_{NG}(SC)$ and $J_{NG}(MPP)$ are smaller than the corresponding geminate losses, meaning that these devices are mainly limited by field-dependent generation. Interestingly, the non-geminate losses are larger for the **P−F** blend, despite the lower coefficient for non-geminate recombination. These larger losses can be rationalized by the rather small charge mobility in this blend, which slows down carrier extraction and makes the photogenerated charge vulnerable to free-carrier recombination. For devices processed with DIO, non-geminate losses are rather insignificant at SC (ca. 10% with regard to J_{gen} at short circuit) but they become relevant at the MPP. Noticeably, the slightly lower mobility of the optimized **P−F** blend is counterbalanced by its lower γ_{BMR}, and non-geminate loss currents are similar in the optimized devices (ca. 24−29% at MPP with respect to $J_{gen}(MPP)$. Therefore, the increase in FF of the DIO-processed blends upon fluorination is mainly caused by a weaker field dependence of the free-carrier generation current and a larger V_{oc}.

Recently, a morphological model was proposed to explain the efficient (and field-independent) free-carrier formation in P3HT:PCBM blends.[65] This model relies on a particular nanomorphology with a less ordered arrangement of the polymer chains at the heterojunction compared to the interior of the P3HT nanocrystallites. By this, polymer chains adjacent to PCBM domains exhibit a lower HOMO and a higher LUMO, forming an energetic barrier for photogenerated holes approaching the fullerene phase and thus slowing down geminate recombination. As shown above by absorption spectroscopy and plasmon mapping, chain aggregation and ordering is clearly improved upon fluorination. Possibly, those domains might possess different degrees of order at the interface and in the interior, causing photogenerated holes to be energetically stabilized away from the heterojunction, preventing rapid geminate recombination. Similar to this, these energetic barriers will also inhibit the intimate contact between free holes and electrons, rendering non-geminate recombination less effective than in a homogeneous 3D donor−acceptor mixture. This is exactly what is seen here, where **P−F** blends with a higher degree of chain aggregation exhibit a smaller Langevin reduction factor.

Though fluorination reduces losses due to geminate and non-geminate recombination, the average IPCE of the optimized **P−F** blend is only 50%, meaning that half of the incident photons are not converted to collected electrons at J_{sc}. A fundamental limit to the IPCE of these devices is that the optimum layer thickness is below 100 nm. Increasing the active layer thickness beyond 100 nm continuously decreased FF, J_{sc}, and PCE, due to inefficient carrier extraction.[16,44] Optical modeling with a transfer matrix formalism revealed that only ∼70% of the incident light is absorbed in an active layer with

dx.doi.org/10.1021/ja305039j | J. Am. Chem. Soc. 2012, 134, 14932−14944

optimum thickness.[44] Also, IPCE spectra are measured at short-circuit conditions. As pointed out above, geminate recombination reduces J_{light} at SC by at least 13%, even for the optimized **P−F** blend. In total, inefficient light absorption and geminate recombination limits the IPCE of this blend to ca. 60%. The IPCE might be further reduced by charge-carrier diffusion to the wrong contact[66] or by extraction of bound PPs at the electrodes.[67] Clearly, further improvement of the IPCE not only requires the application of light trapping schemes or optical spacers[68,69] but also asks for strategies to further reduce geminate and non-geminate losses.

Here, we point out that our study uses polymers of moderate MW ($M_n \approx 10$ kg/mol). It has been shown for other polymer:PCBM blends[9,70−72] that increasing the polymer's MW substantially improves the photovoltaic performance. This phenomena has been related to a concomitant increase of charge-carrier mobility, which promotes charge extraction in competition with non-geminate recombination. In fact, devices made with **P−H** of higher MW ($M_n \approx 17\,000$ g/mol) in our laboratory had EQEs of 2.6 (4.5) when processed without (with) 3% DIO.[44] Very recently (after submission of this manuscript), Jen and co-workers compared the properties of fluorinated PCPDTBT with $M_n = 23\,400$ g/mol with those of regular PCPDTBT of comparable M_n.[73] In a device geometry similar to the one employed by us, their PCPDTBT-based blends processed without an additive gave a PCE of 2.75%, and the efficiency was considerably improved to 5.51% upon fluorination. Although these authors noted that addition of processing additives did not improve PCE further, the combined optimization of the polymer MW, polymer:fullerene blend ratio, and additive concentration might further improve device performance beyond the record efficiency of 6.16% reported here.

Finally, we emphasise that significant improvements of J_{sc} and FF upon fluorine attachment have similarly been reported for other fluorine-substituted copolymers (see Introduction). We therefore propose that the main conclusion of this work—that fluorination improves the solar cell performance not only by increasing the V_{oc} but also by a reduced field dependence of carrier generation and a reduced efficiency for non-geminate recombination—is applicable to most other blend systems comprising F-substituted DA copolymers.

CONCLUSION

In summary, the synthesis and the photovoltaic properties of a new polymer, F-PCPDTBT, designed by fluorination of the BT unit in PCPDTBT, are described. The new polymer gives superior solar cell performance in blends with $PC_{70}BM$. Our measurements show that this enhancement can be mainly attributed to two fundamental effects caused by the fluorination. First, the IE of F-PCPDTBT is 0.1−0.15 eV larger than that of PCPDTBT. This results in a larger energetic difference between the HOMO of the polymer and the LUMO of $PC_{70}BM$, increasing the V_{oc} from 0.61 to 0.74 V. Second, charge-carrier generation becomes more efficient even under reverse bias conditions, and the field dependence of free charge-carrier generation is weakened, meaning that the geminate recombination is strongly reduced. Also, fluorination causes a 3-fold reduction in the non-geminate recombination coefficient at conditions of V_{oc} counterbalancing the reduction in charge-carrier mobility upon fluorine attachment. As a consequence, the FF is increased by 8% and the J_{sc} rises from 11.5 to 14 mA/cm^2 upon fluorine substitution.

We find that the fluorinated polymer has a stronger tendency to aggregate, reducing the optimum amount of processing additive from 3% to 1%. Following arguments put forward to explain the negligible effect of electric field on free charge generation in P3HT:PCBM blends,[65] we assign the superior performance of the optimized F-PCPDTBT:$PC_{70}BM$ blend to the formation of well-ordered polymer aggregates, which stabilizes holes within the hole-transporting polymer phase.

In total, fluorination of PCPDTBT causes the PCE to increase from 3.6% to 6.0% for identical device processing and comparable (medium) molecular weight. Further optimization of the blend ratio and active layer thickness resulted in 6.16% efficiency for F-PCPDTBT:$PC_{70}BM$ solar cells. Our optimized F-PCPDTBT:$PC_{70}BM$ blends clearly outperform the most efficient PCPDTBT:fullerene devices reported so far. As these blends exhibit a high external quantum efficiency of 50% over a broad spectral range, extending from 400 to 800 nm, they are well suited for building the red- to infrared-absorbing subcell of highly efficient polymer tandem solar cells.

ASSOCIATED CONTENT

Supporting Information

Details on the synthesis of the monomers and polymers, sample fabrication and testing, pristine polymer absorption spectra, current voltage characteristics of unipolar devices and OFETs, histograms of the plasmon maps, as well as Q_{tot}, Q_{pre}, and Q_{coll} for different delay times and pre-bias together with the corresponding BMR fits. This material is available free of charge via the Internet at http://pubs.acs.org.

AUTHOR INFORMATION

Corresponding Author

neher@uni-potsdam.de

Notes

The authors declare no competing financial interest.

ACKNOWLEDGMENTS

The authors acknowledge Sybille Allard and Anke Helfer from University of Wuppertal for the high-temperature GPC and Monika Ehlert from University of Potsdam for the TGA measurement. S.J. acknowledges Eileen Katholing for help with the synthesis. W.S. acknowledges Markus Wollgarten for co-work with the TEM data. The work was funded within the BMBF project PVCOMB (FKZ 03IS2151D) and SOHyb (FKZ 03X3525).

REFERENCES

(1) Konarka press release, Feb 28, 2012.
(2) Polyera press release, Feb 1, 2012.
(3) Dou, L.; You, J.; Yang, J.; Chen, C.-C.; He, Y.; Murase, S.; Moriarty, T.; Emery, K.; Li, G.; Yang, Y. *Nat. Photon.* **2012**, *6*, 180−185.
(4) Havinga, E. E.; Tenhoeve, W.; Wynberg, H. *Polym. Bull.* **1992**, *29*, 119−126.
(5) Chen, H.-Y.; Hou, J.; Zhang, S.; Liang, Y.; Yang, G.; Yang, Y.; Yu, L.; Wu, Y.; Li, G. *Nat. Photon.* **2009**, *3*, 649−653.
(6) Chu, T.-Y.; Lu, J.; Beaupré, S.; Zhang, Y.; Pouliot, J.-R. M.; Wakim, S.; Zhou, J.; Leclerc, M.; Li, Z.; Ding, J.; Tao, Y. *J. Am. Chem. Soc.* **2011**, *133*, 4250−4253.
(7) Price, S. C.; Stuart, A. C.; Yang, L.; Zhou, H.; You, W. *J. Am. Chem. Soc.* **2011**, *133*, 4625−4631.
(8) Amb, C. M.; Chen, S.; Graham, K. R.; Subbiah, J.; Small, C. E.; So, F.; Reynolds, J. R. *J. Am. Chem. Soc.* **2011**, *133*, 10062−10065.

(9) Coffin, R. C.; Peet, J.; Rogers, J.; Bazan, G. C. *Nature Chem.* **2009**, *1*, 657−661.
(10) Liang, Y. Y.; Xu, Z.; Xia, J. B.; Tsai, S. T.; Wu, Y.; Li, G.; Ray, C.; Yu, L. P. *Adv. Mater.* **2010**, *22*, E135−E138.
(11) Peet, J.; Kim, J. Y.; Coates, N. E.; Ma, W. L.; Moses, D.; Heeger, A. J.; Bazan, G. C. *Nat. Mater.* **2007**, *6*, 497−500.
(12) Lee, J. K.; Ma, W. L.; Brabec, C. J.; Yuen, J.; Moon, J. S.; Kim, J. Y.; Lee, K.; Bazan, G. C.; Heeger, A. J. *J. Am. Chem. Soc.* **2008**, *130*, 3619−3623.
(13) Chu, T. Y.; Alem, S.; Tsang, S. W.; Tse, S. C.; Wakim, S.; Lu, J. P.; Dennler, G.; Waller, D.; Gaudiana, R.; Tao, Y. *Appl. Phys. Lett.* **2011**, *98*, 3.
(14) Zhu, Z.; Waller, D.; Gaudiana, R.; Morana, M.; Muhlbacher, D.; Scharber, M.; Brabec, C. *Macromolecules* **2007**, *40*, 1981−1986.
(15) Hou, J.; Chen, H.-Y.; Zhang, S.; Li, G.; Yang, Y. *J. Am. Chem. Soc.* **2008**, *130*, 16144−16145.
(16) Scharber, M. C.; Koppe, M.; Gao, J.; Cordella, F.; Loi, M. A.; Denk, P.; Morana, M.; Egelhaaf, H. J.; Forberich, K.; Dennler, G.; Gaudiana, R.; Waller, D.; Zhu, Z. G.; Shi, X. B.; Brabec, C. J. *Adv. Mater.* **2010**, *22*, 367−370.
(17) Gendron, D.; Morin, P. O.; Berrouard, P.; Allard, N.; Aich, B. R.; Garon, C. N.; Tao, Y.; Leclerc, M. *Macromolecules* **2011**, *44*, 7188−7193.
(18) Morana, M.; Azimi, H.; Dennler, G.; Egelhaaf, H.-J.; Scharber, M.; Forberich, K.; Hauch, J.; Gaudiana, R.; Waller, D.; Zhu, Z.; Hingerl, K.; van Bavel, S. S.; Loos, J.; Brabec, C. J. *Adv. Funct. Mater.* **2010**, *20*, 1180−1188.
(19) Kim, J. Y.; Lee, K.; Coates, N. E.; Moses, D.; Nguyen, T. Q.; Dante, M.; Heeger, A. J. *Science* **2007**, *317*, 222−225.
(20) Yang, J.; Zhu, R.; Hong, Z.; He, Y.; Kumar, A.; Li, Y.; Yang, Y. *Adv. Mater.* **2011**, *23*, 3465−3470.
(21) Agostinelli, T.; Ferenczi, T. A. M.; Pires, E.; Foster, S.; Maurano, A.; Müller, C.; Ballantyne, A.; Hampton, M.; Lilliu, S.; Campoy-Quiles, M.; Azimi, H.; Morana, M.; Bradley, D. D. C.; Durrant, J.; Macdonald, J. E.; Stingelin, N.; Nelson, J. *J. Polym. Sci. Part B: Polym. Phys.* **2011**, *49*, 717−724.
(22) Albrecht, S.; Schindler, W.; Kurpiers, J.; Kniepert, J.; Blakesley, J. C.; Dumsch, I.; Allard, S.; Fostiropoulos, K.; Scherf, U.; Neher, D. *J. Phys. Chem. Lett.* **2012**, 640−645.
(23) Lenes, M.; Morana, M.; Brabec, C. J.; Blom, P. W. M. *Adv. Funct. Mater.* **2009**, *19*, 1106−1111.
(24) Blouin, N.; Michaud, A.; Gendron, D.; Wakim, S.; Blair, E.; Neagu-Plesu, R.; Belletete, M.; Durocher, G.; Tao, Y.; Leclerc, M. *J. Am. Chem. Soc.* **2008**, *130*, 732−742.
(25) Hoven, C. V.; Dang, X.-D.; Coffin, R. C.; Peet, J.; Nguyen, T.-Q.; Bazan, G. C. *Adv. Mater.* **2010**, *22*, E63−E66.
(26) Bijleveld, J. C.; Shahid, M.; Gilot, J.; Wienk, M. M.; Janssen, R. A. J. *Adv. Funct. Mater.* **2009**, *19*, 3262−3270.
(27) Liang, Y.; Feng, D.; Wu, Y.; Tsai, S.-T.; Li, G.; Ray, C.; Yu, L. *J. Am. Chem. Soc.* **2009**, *131*, 7792−7799.
(28) Zhang, Y.; Chien, S.-C.; Chen, K.-S.; Yip, H.-L.; Sun, Y.; Davies, J. A.; Chen, F.-C.; Jen, A. K. Y. *Chem. Commun.* **2011**, *47*, 11026−11028.
(29) Babudri, F.; Farinola, G. M.; Naso, F.; Ragni, R. *Chem. Commun.* **2007**, 1003−1022.
(30) Peng, Q.; Liu, X.; Su, D.; Fu, G.; Xu, J.; Dai, L. *Adv. Mater.* **2011**, *23*, 4554−4558.
(31) Zhou, H.; Yang, L.; Stuart, A. C.; Price, S. C.; Liu, S.; You, W. *Angew. Chem., Int. Ed.* **2011**, *50*, 2995−2998.
(32) Son, H. J.; Wang, W.; Xu, T.; Liang, Y.; Wu, Y.; Li, G.; Yu, L. *J. Am. Chem. Soc.* **2011**, *133*, 1885−1894.
(33) Li, Z.; Lu, J.; Tse, S.-C.; Zhou, J.; Du, X.; Tao, Y.; Ding, J. *J. Mater. Chem.* **2011**, *21*, 3226−3233.
(34) Schroeder, B. C.; Huang, Z.; Ashraf, R. S.; Smith, J.; D'Angelo, P.; Watkins, S. E.; Anthopoulos, T. D.; Durrant, J. R.; McCulloch, I. *Adv. Funct. Mater.* **2012**, *22*, 1663−1670.
(35) He, Z.; Zhong, C.; Huang, X.; Wong, W.-Y.; Wu, H.; Chen, L.; Su, S.; Cao, Y. *Adv. Mater.* **2011**, *23*, 4636−4643.
(36) Lange, A.; Krueger, H.; Ecker, B.; Tunc, A. V.; von Hauff, E.; Morana, M. *J. Polym. Sci. Part A: Polym. Chem.* **2012**, *50*, 1622−1635.
(37) Pilgram, K.; Zupan, M.; Skiles, R. *J. Heterocycl. Chem.* **1970**, *7*, 629−633.
(38) Peet, J.; Cho, N. S.; Lee, S. K.; Bazan, G. C. *Macromolecules* **2008**, *41*, 8655−8659.
(39) Rogers, J. T.; Schmidt, K.; Toney, M. F.; Bazan, G. C.; Kramer, E. J. *J. Am. Chem. Soc.* **2012**, *134*, 2884−2887.
(40) Herzing, A. A.; Richter, L. J.; Anderson, I. M. *J. Phys. Chem. C* **2010**, *114*, 17501−17508.
(41) Schindler, W.; Wollgarten, M.; Fostiropoulos, K. *Org. Electron.* **2012**, *13*, 1100−1104.
(42) Rogers, J. T.; Schmidt, K.; Toney, M. F.; Kramer, E. J.; Bazan, G. C. *Adv. Mater.* **2011**, *23*, 2284−2288.
(43) Gu, Y.; Wang, C.; Russell, T. P. *Adv. Energy Mater.* **2012**, *2*, 683−690.
(44) Albrecht, S.; Schäfer, S.; Lange, I.; Yilmaz, S.; Dumsch, I.; Allard, S.; Scherf, U.; Hertwig, A.; Neher, D. *Org. Electron.* **2012**, *13*, 615−622.
(45) Chen, H.-Y.; Hou, J.; Hayden, A. E.; Yang, H.; Houk, K. N.; Yang, Y. *Adv. Mater.* **2010**, *22*, 371−375.
(46) Kniepert, J.; Schubert, M.; Blakesley, J. C.; Neher, D. *J. Phys. Chem. Lett.* **2011**, *2*, 700−705.
(47) Hwang, I. W.; Soci, C.; Moses, D.; Zhu, Z.; Waller, D.; Gaudiana, R.; Brabec, C. J.; Heeger, A. J. *Adv. Mater.* **2007**, *19*, 2307−2312.
(48) Jarzab, D.; Cordella, F.; Gao, J.; Scharber, M.; Egelhaaf, H.-J.; Loi, M. A. *Adv. Energy Mater.* **2011**, *1*, 604−609.
(49) Etzold, F.; Howard, I. A.; Forler, N.; Cho, D. M.; Meister, M.; Mangold, H.; Shu, J.; Hansen, M. R.; Mullen, K.; Laquai, F. *J. Am. Chem. Soc.* **2012**, *134*, 10569−10583.
(50) Yamamoto, S.; Ohkita, H.; Benten, H.; Ito, S. *J. Phys. Chem. C* **2012**, *116*, 14804−14810.
(51) Maurano, A.; Hamilton, R.; Shuttle, C. G.; Ballantyne, A. M.; Nelson, J.; O'Regan, B.; Zhang, W.; McCulloch, I.; Azimi, H.; Morana, M.; Brabec, C. J.; Durrant, J. R. *Adv. Mater.* **2010**, *22*, 4987−4992.
(52) Carsten, B.; Szarko, J. M.; Son, H. J.; Wang, W.; Lu, L.; He, F.; Rolczynski, B. S.; Lou, S. J.; Chen, L. X.; Yu, L. *J. Am. Chem. Soc.* **2011**, *133*, 20468−20475.
(53) Koster, L. J. A. *Phys. Rev. B* **2010**, *81*, 205318.
(54) Bange, S.; Schubert, M.; Neher, D. *Phys. Rev. B* **2010**, *81*, 035209.
(55) Cho, S.; Lee, J. K.; Moon, J. S.; Yuen, J.; Lee, K.; Heeger, A. J. *Org. Electron.* **2008**, *9*, 1107−1111.
(56) Dieckmann, A.; Bassler, H.; Borsenberger, P. M. *J. Chem. Phys.* **1993**, *99*, 8136−8141.
(57) Pivrikas, A.; Juska, G.; Mozer, A. J.; Scharber, M.; Arlauskas, K.; Sariciftci, N. S.; Stubb, H.; Osterbacka, R. *Phys. Rev. Lett.* **2005**, 94.
(58) Deibel, C.; Wagenpfahl, A.; Dyakonov, V. *Phys. Rev. B* **2009**, *80*, 075203.
(59) Groves, C.; Greenham, N. C. *Phys. Rev. B* **2008**, *78*, 155205.
(60) Deibel, C.; Baumann, A.; Dyakonov, V. *Appl. Phys. Lett.* **2008**, 93.
(61) Hamilton, R.; Shuttle, C. G.; Oâ€Regan, B.; Hammant, T. C.; Nelson, J.; Durrant, J. R. *J. Phys. Chem. Lett.* **2010**, *1*, 1432−1436.
(62) Mauer, R.; Howard, I. A.; Laquai, F. d. r. *J. Phys. Chem. Lett.* **2010**, *1*, 3500−3505.
(63) Howard, I. A.; Mauer, R.; Meister, M.; Laquai, F. *J. Am. Chem. Soc.* **2010**, *132*, 14866−14876.
(64) Guo, J. M.; Ohkita, H.; Benten, H.; Ito, S. *J. Am. Chem. Soc.* **2010**, *132*, 6154−6164.
(65) McMahon, D. P.; Cheung, D. L.; Troisi, A. *J. Phys. Chem. Lett.* **2011**, *2*, 2737−2741.
(66) Sokel, R.; Hughes, R. C. *J. Appl. Phys.* **1982**, *53*, 7414−7424.
(67) Strobel, T.; Deibel, C.; Dyakonov, V. *Phys. Rev. Lett.* **2010**, 105.
(68) You, J.; Li, X.; Xie, F.-x.; Sha, W. E. I.; Kwong, J. H. W.; Li, G.; Choy, W. C. H.; Yang, Y. *Adv. Energy Mater.* **2012**, DOI: 10.1002/aenm.201200108.

(69) Wang, D. H.; Park, K. H.; Seo, J. H.; Seifter, J.; Jeon, J. H.; Kim, J. K.; Park, J. H.; Park, O. O.; Heeger, A. J. *Adv. Energy Mater.* **2011**, *1*, 766−770.
(70) Tong, M.; Cho, S.; Rogers, J. T.; Schmidt, K.; Hsu, B. B. Y.; Moses, D.; Coffin, R. C.; Kramer, E. J.; Bazan, G. C.; Heeger, A. J. *Adv. Funct. Mater.* **2010**, *20*, 3959−3965.
(71) Schilinsky, P.; Asawapirom, U.; Scherf, U.; Biele, M.; Brabec, C. J. *Chem. Mater.* **2005**, *17*, 2175−2180.
(72) Ma, W.; Kim, J. Y.; Lee, K.; Heeger, A. J. *Macromol. Rapid Commun.* **2007**, *28*, 1776−1780.
(73) Zhang, Y.; Zou, J.; Cheuh, C.-C.; Yip, H.-L.; Jen, A. K. Y. *Macromolecules* **2012**, *45*, 5427−5435.